Annalen der Physik. 7. Folge, Band 47, Heft 8, 1990, S. 635–648 J. A. Barth, Leipzig

A Clear Atomic Example for the Surface Sensitivity of Penning Ionization: $He^*(2^3S)$ + Yb

By H. Hotop, M.-W. Ruf and A. J. Yencha

Fachbereich Physik, Universität Kaiserslautern, Kaiserslautern, FRG

B. Fricke

Fachbereich Physik, Universität/GHS Kassel, Kassel, FRG

Den Annalen der Physik zum 200. Geburtstag gewidmet

Abstract. Using a crossed-beam apparatus with a double hemispherical electron spectrometer, we have studied the spectrum of electrons released in thermal energy ionizing collisions of metastable $He^*(2^3S)$ atoms with ground state $Yb(4f^{14}\,6s^2\,{}^1S_0)$ atoms, thereby providing the first Penning electron spectrum of an atomic target with 4f-electrons. In contrast to the HeI (58.4 nm) and NeI (73.6/74.4 nm) photoelectron spectra of Yb, which show mainly 4f- and 6s-electron emission in about a 5:1 ratio, the $He^*(2^3S)$ Penning electron spectrum is dominated by 6s-ionization, accompanied by some correlation-induced 6p-emission (8% $Yb^+(4f^{14}\,6p\,{}^2P)$ formation) and very little 4f-ionization ($\lesssim 2.5\%$). This astounding result is attributed to the electron exchange mechanism for $He^*(2^3S)$ ionization and reflects the poor overlap of the target 4f-electron wavefunction with the 1s-hole of $He^*(2^3S)$, as discussed on the basis of Dirac-Fock wave functions for the Yb orbitals and through calculations of the partial ionization cross sections involving semiempirical complex potentials. The presented case may be regarded as the clearest atomic example for the surface sensitivity of $He^*(2^3S)$ Penning ionization observed so far.

Ein klares atomares Beispiel für die Oberflächenempfindlichkeit der Penning-Ionisation: $He^*(2^3S)$ + Yb

Inhaltsübersicht. Unter Benutzung einer Kreuzstrahl-Apparatur mit Doppelhalbkugel-Elektronenspektrometer haben wir das Energiespektrum von Elektronen untersucht, die bei thermischen, ionisierenden Stößen von metastabilen $He^*(2^3S)$-Atomen mit $Yb(4f^{14}6s^2\,{}^1S_0)$ Atomen im Grundzustand freigesetzt werden; damit liegt erstmals ein Penning-Elektronenspektrum eines Atoms mit 4f-Elektronen vor. Im Gegensatz zu den HeI (58.4 nm) und NeI (73.6/74.4 nm) Photoelektronenspektren von Yb, die vor allem die Emission von 4f- und 6s-Elektronen im Verhältnis von etwa 5:1 zeigen, dominiert im $He^*(2^3S)$ Penning-Elektronenspektrum die 6s-Ionisation, die von 8% $Yb^+(4f^{14}\,6p\,{}^2P)$-Bildung und sehr geringer 4f-Ionisation ($\lesssim 2.5\%$) begleitet wird. Dieses erstaunliche Ergebnis erklären wir mit dem Elektronenaustausch-Mechanismus für die $He^*(2^3S)$ Penning-Ionisation; es spiegelt den geringen Überlapp der Yb(4f)-Elektronen mit dem 1s-Loch in $He^*(2^3S)$ wider, wie anhand von Modellrechnungen auf der Basis semiempirischer komplexer Wechselwirkungspotentiale verdeutlicht wird. Das hier untersuchte Stoßsystem stellt ein besonders klares atomares Beispiel für die Oberflächenempfindlichkeit der Penning-Ionisation durch $He^*(2^3S)$-Atome dar.

1. Introduction

One of the interesting questions in the ionization of a multielectron atom or molecule is how the response of the system is distributed among the various subshells. In photoionization, it is well-known [1] that electric dipole-matrix elements may change sign at particular energies, yielding "Seaton-Cooper" minima in the cross sections for ionization of a particular orbital and correspondingly enhance the contribution of other orbitals to the total ionization cross section. Often, however, the relative strength of the ionization cross sections of outer orbitals with similar binding energies will reflect the orbital occupancy in a way, which depends rather weakly on the photon energy. An example for the former situation is the HeI (58.4 nm) photoelectron spectrum of $Hg(5d^{10}\,6s^2\,{}^1S_0)$, which is dominated by 5d-emission [2, 3], exceeding the suppressed 6s-channel by a factor of about 30 (instead of 5 expected from the orbital occupancies). As an example for the latter situation, we mention the HeI (58.4 nm) and NeI (73.6/74.4 nm) photoelectron spectra of $Yb(4f^{14}\,6s^2\,{}^1S_0)$, which mainly show 4f- and 6s-emission in about a 5:1 ratio (rather close to the 7:1 orbital occupancy) [4, 5].

Compared with photoionization, ionization of target species X induced in thermal energy collisions with excited atoms A* (Penning ionization) [6—9]

$$A^* + X \rightarrow A + X^+ + e^-(E) \tag{1}$$

is known to be governed by a different transition mechanism, if the energy carriers are metastable species such as $He^*(2^3S)$ or $He^*(2^1S)$. One of the first atomic targets studied by Penning ionization electron spectrometry (PIES) was Hg [10, 11], and it was found for $He^*(2^3S)$ ionization — contrast to HeI photoionization — that 6s-removal occurred with a probability about 50% larger than the one for 5d-removal. Hotop and Niehaus associated this finding with their exchange model description of the Penning process [11], according to which ionization proceeds through transfer of an electron from the target species X into the 1s-vacancy in He* accompanied by emission of the 2s-electron from He*. It is clear that in the electron exchange model the overlap of the target electrons with the core hole of the excited atom plays a crucial role [9, 11—14], and this is in fact reflected in the local autoionization width function $\Gamma(R)$, which describes the coupling of the autoionizing quasi-molecule $A^* + X$ to the continuum $(A + X^*) + e^-(E)$ state [12—16]. So far, quantitative analyses, based on ab initio local complex potentials $V_c(R) = V^*(R) - i\Gamma(R)/2$ for the entrance channel $A^* + X$, have only been carried out for the simplest PI-systems, e.g. $He^*(2^3S) + H$ [15—20], $He^*(2^3S) + Li$ [19—21], and $He^*(2^3S) + Na$ [19, 20, 22, 23]. It would, however, be desirable to gain a deeper understanding also for systems with several different exit channels such as $He^*(2^3S) + Hg$ and to extend the experimental studies to target species, which offer orbitals for ionization with strongly different spatial extensions, yet have a simple level structure both in the neutral and ionized state.

The ytterbium atom promises to be a suitable candidate. With closed 4f- and 6s-outer shells it possesses a ${}^1S_0$ ground state; the HeI- or NeI-photoelectron spectra are dominated by 6s- and 4f-removal [4, 5], leading to $Yb^+(4f^{14}\,6s^1\,{}^2S_{1/2})$ and $Yb^+(4f^{13}\,6s^2\,{}^2F_{7/2,5/2})$ ionic states with binding energies of 6.254 eV and 8.910/10.168 eV, respectively. While the 6s- and 4f-binding energies are quite similar, their radial expectation values differ drastically ($\langle r\rangle_{6s} = 3.9\,a_0$, $\langle r\rangle_{4f} \approx 0.74\,a_0$ [24]). The essential aspects of the orbital extensions in $He^*(2^3S) + Yb$ collisions are illustrated in Fig. 1.

The lower part of Fig. 1 shows the radial electron density distributions for the 4f-, 6s-, and 6p-orbitals in the ground state $Yb({}^1S_0)$ atom, as obtained in a Multiconfiguration Dirac Fock calculation (see section 3.2). For an internuclear separation $R = 7\,a_0$ (close to the equilibrium distance R_{e^*} of the $He^*(2^3S) + Yb({}^3\Sigma)$ entrance channel potential curve), the upper part of Fig. 1 presents a simple planar view of the system including

circles to indicate the radial expectation values of the respective atomic orbitals. It is obvious that for $R \gtrsim 5\ a_0$ the overlap of the 4f-electrons with the 1s-hole in He*(2^3S) is small compared to that of the 6s-electrons. Correspondingly, one may expect relatively little ionization involving 4f-removal, but dominant 6s-ionization, reflecting a high "surface sensitivity" of the Penning process, which is of substantial interest in connection with studies of solid and liquid surfaces by metastable atom impact [25—28].

In this paper, we present for the first time a Penning ionization electron spectrum of Yb; it in fact clearly exhibits the anticipated behaviour, which is particularly striking in comparison with the HeI or NeI photoelectron data. By classical calculations, involving estimated complex potentials, we address the problem, how the autoionizing He*(2^3S) +

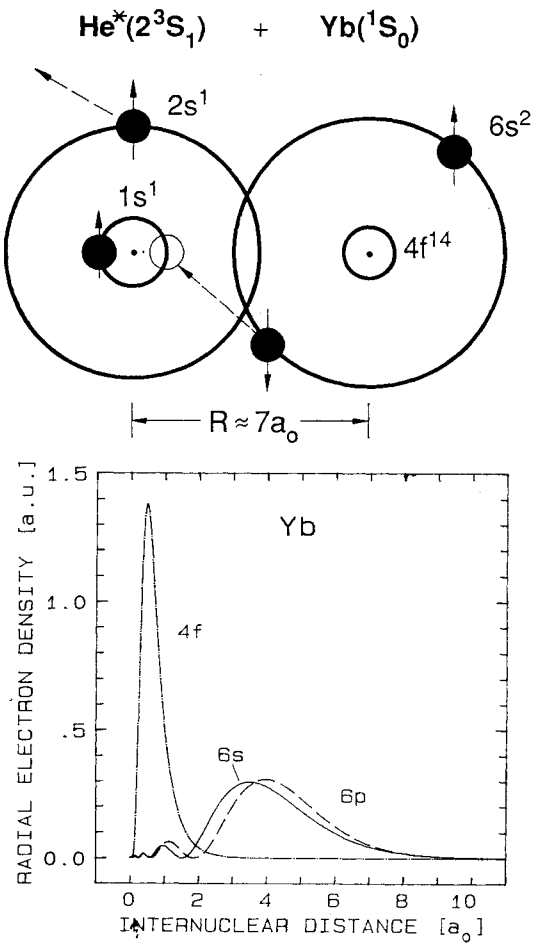

Fig. 1. Illustration of the electron exchange process leading to Penning ionization of Yb-atoms in collisions with He*(2^3S) atoms (upper part). The radial electron density distributions in the Yb-atom (normalized to one electron per orbital) for the $4f^{14}$- and the $6s^2$-shell together with its $6p^2$-admixture are shown in the lower part of the figure. For clarity, only the $6p_{3/2}$ and $4f_{5/2}$ radial density functions are shown; on the displayed scales, they are nearly identical to those of $6p_{1/2}$ and $4f_{7/2}$, respectively

Yb system is coupled to the different exit channels, and shed light on the R-dependent partial autoionization probabilities and their collision energy dependence. In this way, the "surface sensitivity" of Penning ionization is put on a quantitative basis.

2. Experimental

The PIES apparatus, used in the present work, is identical to the one described previously in connection with an electron spectrometric study of He*(2^3S, 2^1S) + alkali atom collisions [29]. Briefly, a collimated metastable He*(2^3S, 2^1S) beam from a differentially-pumped dc discharge source crosses a collimated Yb atom beam from a resistively-heated, differentially-pumped metal vapour oven in a magnetically-shielded, field-free region. Electrons released in ionizing collisions between the two beams are sampled in a direction perpendicular to both beams and imaged onto the entrance slit of a double hemispherical condenser, operating at a pass energy of 9.6 eV and a nominal resolution of 36 meV (FWHM). The electrons are detected with a channel multiplier and fast counting electronics. Multichannel scaling techniques are used to generate the electron energy spectra. The energy scale and the effective energy resolution (including surface potential variations) are determined by simultaneously measuring the well-known spectra of Ar or Xe atoms, which are admitted to the reaction region at a suitable small density. The metastable He* beam has supersonic character with an average velocity $\bar{v}_{He} = 1750$ m/s and a velocity width $\Delta v/\bar{v}_{He}$ (FWHM) of 31% [29]. From this and the effusive beam velocity distribution of the crossed Yb atoms ($T_{Yb} \approx 1000$ K), the relative collision energy distribution of Table 1 has been calculated, yielding an average collision energy $\bar{E}_{rel} = 66$ meV. The mixed, metastable He*(2^3S, 2^1S) beam, containing about 7 times more He*(2^3S) than He*(2^1S) atoms [29], was state-selected by irradiation from a helical, cooled He discharge, surrounding the He* beam for about 5 cm, resulting in effective (>99%) and selective removal of He*(2^1S) atoms [18, 29]. In this paper, we only present He*(2^3S) data; the He*(2^1S) results will be included in a future publication, which discusses the interaction of metastable He*(2^3S, 2^1S) atoms with Mg, Ca, Sr, Ba, and Yb atoms.

Table 1. Distribution $f(E_{rel})$ of relative collision energies for He*(2^3S) + Yb collisions, as used in the calculation of partial, energy averaged ionization cross sections (cf. Table 2)

E_{rel} [meV]	30	40	50	60	70	80	90	100	110	120
$f(E_{rel})$ [%]	1.53	7.18	17.17	24.06	22.41	15.10	7.80	3.23	1.11	0.41

3. Results and Discussion

3.1. Comparison of VUV Photoelectron and He*(2^3S) Penning Electron Spectra of Yb

In Fig. 2, we present our He*(2^3S) + Yb spectrum and show for comparison the HeI photoelectron spectrum in the binding energy range 5—13 eV, as obtained by Lee et al. [4]. The latter spectrum is dominated by three peaks, which correspond to simple removal of an electron from the $6s_{1/2}$, $4f_{7/2}$, and $4f_{5/2}$ orbitals, respectively. Formation of the excited ionic states $Yb^+(4f^{14}\,6p_{1/2,3/2})$ and $Yb^+(4f^{14}\,5d_{3/2,5/2})$, induced by correlation effects, is a weak process. The Penning electron spectrum is strongly dominated by simple 6s-removal, which accounts for about 90% of the intensity in the energy range covered in Fig. 2. At a magnification of a factor of 10, the two peaks due to correlation-induced

$Yb^+(4f^{14}\ 6p_{1/2,3/2})$ formation come out clearly, and in their neighbourhood to lower and higher electron energies weak, rather broad features are observed, which we associate with $4f_{5/2}$- and $4f_{7/2}$-removal (the latter possibly containing intensity due to $Yb^+(4f^{14}\ 5d)$ formation).

In Table 2, we summarize the intensities (peak areas) observed in the $He^*(2^3S)$ + Yb spectrum and compare them with results obtained in HeI (58.4 nm) and NeI (73.6 nm) photoionization by Lee et al. [4] and Kerling et al. [5]. The 6s:4f branching ratio is

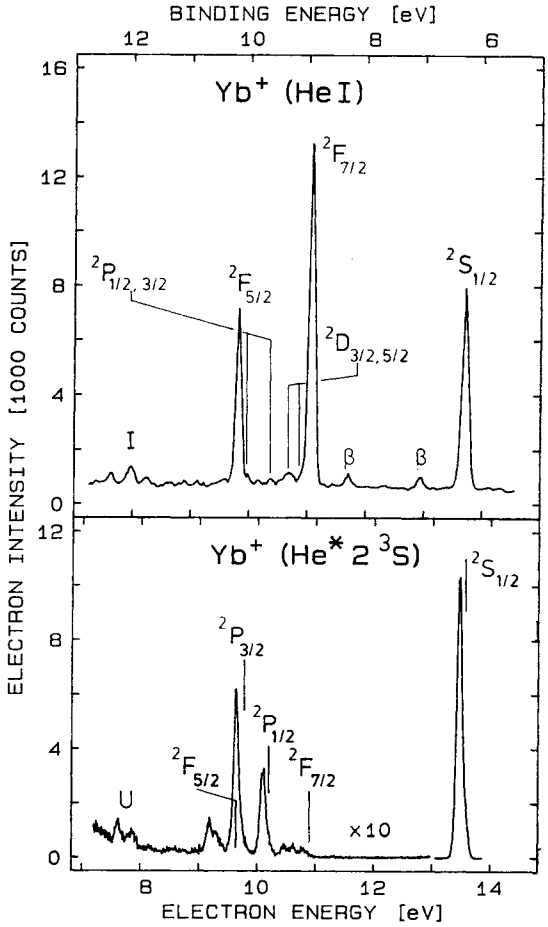

Fig. 2. Comparison of HeI (58.4 nm) photoelectron spectrum of ground state $Yb(^1S_0)$ atoms (redrawn from Fig. 4 of ref. [4] with permission) with $He^*(2^3S)$ Penning ionization electron spectrum of $Yb(^1S_0)$, measured in this work; note the 10 fold sensitivity increase in the intensity scale of the $He^*(2^3S)$ spectrum for energies below 13 eV. In the HeI spectrum, the peaks labelled "β" are due to 4f-ionization by HeI_β (53.7 nm) light, the peak labelled "I" is attributed to inelastically scattered electrons (see ref. [4]). The HeI spectrum shows "satellite" peaks at binding energies above 11.7 eV (see refs. [4, 5] for details); the peaks labelled "U" in the $He^*(2^3S)$ spectrum are likely due to "satellites". In the $He^*(2^3S)$ spectrum the different peaks are more or less strongly shifted away from the respective "nominal" energies E_0 (vertical lines) towards lower energies due to the influence of the interatomic potentials in the entrance and exit channels (E_0 = excitation energy of $He^*(2^3S)$ minus respective binding energy)

found to be drastically different in photoionization and Penning ionization: whereas in HeI/NeI photoionization, the cross section ratio $Q_{4f}:Q_{6s} \approx 5$ is rather close to the ratio of the orbital occupancy (7:1), it is more than 100 times smaller in Penning ionization. On the other hand, the cross section ratio $Q_{6p}:Q_{6s}$ is rather similar in photo- and Penning ionization and quite close to the relative admixture of the $(6p)^2$ configuration to the dominant $(6s)^2$ configuration, as found in a relativistic CI description of the outer valence shell (see section 3.2).

Table 2. Relative population of Yb^+ ionic states formed in HeI and NeI photoionization and $He^*(2^3S)$ Penning ionization of ground state Yb $^1S_0$) atoms

Projectile	Ref.	Relative population of Yb^+ states				
		$6s\ ^2S_{1/2}$	$6p\ ^2P_{1/2}$	$6p\ ^2P_{3/2}$	$4f^{13}\ ^2F_{7/2}$	$4f^{13}\ ^2F_{5/2}$
HeI (58.4 nm)	a	100	3 (3)	5 (—)	180 (251)	95 (134)
	b	100	6.4 ± 2.2	—	296 ± 22	165 ± 18
NeI (73.6 nm)	a	100	3	5	281 (356)	135 (164)
	b	100	7.4 ± 1.5	10.0 ± 2.0	402 ± 29	193 ± 21
$He^*(2^3S)$	c	100	3.2	5.6	1.0	1.8
		100	8.8 + 0.1 −1.4		2.8 + 0.1 − 0.6	
	d	100	7.80		2.96	

a) ref. [4], data obtained at $\vartheta = 90°$ with respect to unpolarized photon beam and corrected for theoretical spectrometer transmission function. The values in brackets have been corrected for photoelectron angular distribution by use of β-parameters from ref. 5

b) ref. [5], data corrected for photoelectron angular distribution, not corrected for spectrometer transmission function (in the electron energy range studied, the transmission correction is estimated to be below 20%)

c) present experiment, the correction for angular distribution effects is likely below 10% (For the similar system $He^*(2^3S)$ + Hg almost isotropic intensity distributions were observed [43]). Data not corrected for spectrometer transmission function, upper error limits due to counting statistics, lower error limits due to estimated maximum transmission correction

d) present model calculation; collision energy averaged cross sections $\bar{Q}_k$ are given, calculated by $\bar{Q}_k = \int_0^\infty Q_k(E_{rel}) f(E_{rel})\, dE_{rel}$, using the normalized collision energy distribution $f(E_{rel})$ of Table 1

The photoionization results are "simple" in the sense that the observed intensities essentially reflect the overall densities of the ionized electrons in the Yb atom. How can the very low 4f-ionization probability in $He^*(2^3S)$ + Yb collisions be understood?

As suggested by Fig. 1, electron exchange from the compact 4f-orbital to the compact 1s-hole in $He^*(1s2s^3S)$ will be unlikely at typical internuclear distances $R \gtrsim 5\, a_0$, in contrast to electron exchange from the extended 6s-orbital and from the admixed 6p-orbital (which is slightly larger than 6s, see Fig. 1). In an attempt to quantify this qualitative expectation, we have carried out classical model calculations of the partial Penning ionization cross sections, taking into account the R-dependent coupling to the various final ionic states and the heavy particle dynamics of the system. These calculations will be described in section 3.2.

Apart from yielding the partial ionization cross sections, the Penning electron spectrum contains rather detailed information on the molecular interactions in the $He^*(2^3S)$ + $Yb(^3\Sigma)$ entrance channel potential curve $V^*(R)$ and on the He + Yb^+ exit channel potentials $V^+(R)$. As clearly observed in Fig. 2, the Penning electron peaks are shifted to lower electron energies relative to their respective "nominal" energy

E_0 = excitation energy of He*(2^3S) minus respective Yb-binding energy. This shift to lower energies indicates a sizeable attraction in the entrance channel $V^*(R)$ [6—8, 11, 29—31]. A characteristic energy position is the low energy edge E_* [6—8, 29—31], i.e. the point at which the intensity has dropped to 43.8% of the peak intensity towards lower energy. In a semiclassical description of the electron energy spectrum, the low energy peak can be described by the square of an Airy function [6—8, 31] and the point E_* is directly related to an extremum (here a minimum) in the local electron energy function $E(R) = V^*(R) - V^+(R)$ at some distance $\hat{R}$ by $E_* = V^*(\hat{R}) - V^+(\hat{R})$.

Without going into too much detail, an inspection of the different Penning electron peaks in Fig. 2 leads to the following conclusions:

i) the well depth D_e^* of the He*(2^3S) + Yb($^3\Sigma$) potential, extracted from the edge position E_* of the Yb^+(6s)-peak ($E_0 - E_* = 150$ meV) is about 160 meV (see section 3.2).

ii) the edge shift of the $Yb^+(6p_{3/2})$ peak ($E_0 - E_* = 206$ meV) is larger than for Yb^+(6s) and for $Yb^+(6p_{1/2})$ ($E_0 - E_* = 155$ meV), pointing to differences between the respective ionic potentials in the R-range, in which ionization occurs. For $Yb^+(6p_{3/2})$, we associate the increased shift with transitions to the basically repulsive He + $Yb^+(6p_{3/2})$ $^2\Sigma$ potential curve.

iii) The peak at about 9.2 eV electron energy is attributed to formation of the $Yb^+(4f^{13}{}_{5/2}\ 6s^2)$ state (no other designation appears likely to us); its edge shift amounts to $E_0 - E_* = 524$ meV, much larger than for 6s and 6p. This behaviour, however, is consistent with the idea that the autoionization coupling to the 4f-channel only becomes substantial at smaller R, for which the He + $Yb^+(4f^{13}{}_{5/2}\ 6s^2)$ potential is well in the repulsive part.

3.2. Semiempirical Construction of a Local Complex Potential for He*(2^3S) + Yb

Within the local complex potential description of Penning ionization [6—9, 12, 14—23, 31, 32] one has to know the real part $V^*(R)$ of the He*(2^3S) + Yb($^3\Sigma$) potential, in which the heavy particles move, and the partial autoionization widths functions $\Gamma_k(R)$, which describe the coupling to exit channels k and add up to the total width $\Gamma(R) = \sum_k \Gamma_k R)$. None of these quantities is so far known for He*(2^3S) + Yb. Based on the present knowledge of other systems and experience, we therefore construct semi-empirically functions $V^*(R)$ and $\Gamma_k(R)$, which we consider to represent a reasonable choice. In section 3.3, we shall use these functions in a classical calculation to obtain R-dependent differential cross sections $q_k(R)$, integrated partial cross sections $Q_k = \int_0^\infty q_k(R)\,\mathrm{d}R$, and ionization probabilities (opacities) over the collision energy range $10\ \mathrm{meV} \leq E_{\mathrm{rel}} \leq 500\ \mathrm{meV}$.

In constructing the real part $V^*(R)$ of the He*(2^3S) + Yb($^3\Sigma$) potential, we use the chemical equivalence of the He*(2^3S) atom with the Li(2^2S) atom [6—8, 11, 15, 29] and similarities between the Yb atom and the Ca atom and — to a lesser extent — with the Hg atom. We note that — to our knowledge — no experimental or theoretical potentials for Li + Yb or He*(2^3S) + Yb are known so far. From our PIES data for the Yb^+(6s) peak (section 3.1), we derive a well depth for the He*(2^3S) + Yb potential of $D_e^* = 160(20)$ meV, using formula (4) in ref. [29] and an estimated value $-V^+(R_e^*) = 10$ meV at $R_e^* = 6.8\ a_0$. The equilibrium distance $R_e^* = 6.8\ a_0$ is chosen on the following basis. According to an ab initio calculation of the Li(2^2S) + Ca($^2\Sigma$) potential [33], its R_e is 6.7 a_0; since the radii of the outer shell electrons in Ca($4s^2$) and Yb($6s^2$) [24] as well as the polarizabilities of Ca and Yb [34] are in close agreement, one expects that the equilibrium distance of the Li(2^2S) + Yb potential is close to the one for Li(2^2S) + Ca,

i.e. 6.7 a_0. Such a value is also supported by the well-known potential for Li(2^2S) + Hg ($R_e = 5.67\ a_0$), determined by inversion of elastic scattering data [35], in combination with the known difference (1.2 a_0) between the radial expectation values of the 6s-orbitals in Yb and Hg [24]. The R_e^* value for the He*(2^3S) + Yb potential should be slightly larger than for Li(2^2S) + Yb according to previous observations for the interaction of He*(2^3S) and Li(2^2S), respectively, with the same target atom [29]; therefore, we use $R_e^* = 6.8\ a_0$. For the shape of the He*(2^3S) + Yb potential, we take the reduced form of the Li(2^2S) + Hg interaction [35].

The autoionization widths are modelled according to our observation that the R-dependence of accurate ab initio widths functions $\Gamma(R)$ for He*(2^3S) + H, Li, Na [19, 20] as well as of experimentally determined widths for He*(2^3S) + Ar [36] is found to agree quite well over a large range of $r = R$ with the radial electron density distribution $\varrho(r) \sim r^2\ |F(r)|^2$ of the respective target radial wave function $F(r)$, i.e. we set

$$\Gamma_k(R) = c_k R^2\ |F_k(R)|^2. \tag{2}$$

The constant c_k is found to be rather strongly dependent on the size of the considered orbital $F_k(r)$ and therefore a critical parameter. For Yb($6s^2$), we fix c_{6s} by comparison of the ab initio $\Gamma(R)$ for He*(2^3S) + Na(3s) [20] with the Na(3s) Hartree-Fock wave function [37]; for Yb($4f^{14}$), c_{4f} is chosen (for both, $4f_{5/2}$ and $4f_{7/2}$) by comparison of $\Gamma(R)$ for He*(2^3S) + Ar [36] with the Hartree-Fock wave function for Ar($3p^6$) [37] with

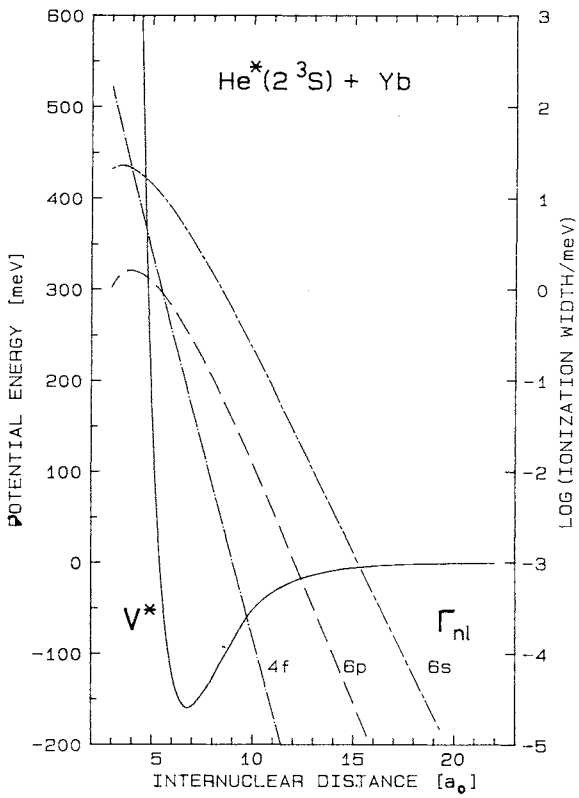

Fig. 3. Interatomic potential $V^*(R)$ and partial autoionization width functions $\Gamma_{nl}(R)$ for the system He*(2^3S) + Yb($^1S_0$), constructed as described in the text and used in model calculations of total and partial ionization cross sections (Figs. 4–6)

emphasis on the region around $r = R \approx 6\,a_0$. The width for the coupling to the $Yb^+(6p)$ exit channel was chosen according to the admixture of $(6p)^2$ (average of $(6p_{3/2})^2$ and $(6p_{1/2})^2$) to $(6s)^2$, as obtained in our Multiconfiguration Dirac-Fock calculation, which we describe briefly at the end of this section.

In Fig. 3, we show the functions $V^*(R)$ and $\Gamma_k(r)$ for the $He^*(2^3S) + Yb$ system, constructed above. As was qualitatively clear from the diagrams in Fig. 1, the coupling to the $Yb^+(^2F)$ ionic channel will play a significant role only for small internuclear separations. The calculations in section 3.3 will quantify this insight.

For the calculation of the electron wave function of the ground state $Yb(J = 0^+)$ atom we used a relativistic Multiconfiguration Dirac Fock atomic structure program [38]. In order to account for correlation effects in the valence shell, we took all possible configurations which can be constructed by distributing two electrons in the five outer shells 6s, $6p_{1/2}$, $6p_{3/2}$, $5d_{3/2}$, and $5d_{5/2}$. During the self consistent procedure these single particle functions as well as the weights of the configurations are varied in such a way that the total energy becomes a minimum. The use of a relativistic code is necessary because relativistic effects affect the wave functions strongly. For example, the 6s and $6p_{1/2}$ wave functions are contracted by about 15% as compared to a non-relativistic treatment and thus influence, via the self consistent treatment, all other outer electron wave functions, too. As optimized weights of the five valence shell configurations we obtained: $6s^2$:93.5%; $6p_{1/2}^2$:2.5%; $6p_{3/2}^2$:3.5%; $5d_{3/2}^2$:0.16%; $5d_{5/2}^2$:0.34%. The admixture of $6p^2$ amounts to 6.4% relative to $6s^2$, whereas the $5d^2$ contribution (0.53%) is so weak that it was neglected in the autoionization width.

3.3. Model Calculations of the Partial Penning Ionization Cross Sections

In this section, we describe classical calculations of the partial cross sections $q_k(R)$ and $Q_k = \int_0^\infty q_k(R)\mathrm{d}R$. First, we briefly describe the classical formulae, which are the basis of our cross section calculations. The differential cross section $q(R)$ for total autoionization per unit radial distance in the interval $(R, R + \mathrm{d}R)$ is given by [15, 31]

$$q(R) = (\pi\hbar^2/2\mu E_{\mathrm{rel}}) \sum_{J=0}^{\infty} (2J + 1)\, P_J(R), \tag{3}$$

E_{rel} = relative collision energy; μ = reduced mass; J = orbital angular momentum quantum number of heavy particle motion; $\hbar = h/2\pi$ = Planck's constant. The J-dependent differential autoionization probability $P_J(R)$ is obtained from [15]

$$P_J(R) = 2w_J(R) \cdot \exp\left[-\int_{R_{t_J}}^{\infty} w_J(R')\,\mathrm{d}R'\right] \cdot \cosh\left[\int_{R_{t_J}}^{R} w_J(R')\,\mathrm{d}R'\right], \tag{4}$$

where R_{t_J} is the classical turning point and $w_J(R) = \Gamma(R)/\hbar v_J(R)$ is the total single passage differential autoionization probability without the consideration of prior loss of flux ($v_J(R)$ = radial velocity). According to (4), $P_J(R)$ can be interpreted as the product of an effective survival factor $S_J^{\mathrm{eff}}(R)$

$$S_J^{\mathrm{eff}}(R) = \exp\left[-\int_{R_{t_J}}^{\infty} \mathrm{d}R'\; \Gamma(R')/\hbar v_J(R')\right] \cdot \cosh\left[\int_{R_{t_J}}^{R} \mathrm{d}R'\; \Gamma(R')/\hbar v_J(R')\right], \tag{5}$$

with twice the differential autoionization probability $w_J(R)$ (corresponding to inward plus outward passage along the trajectory)

$$P_J(R) = 2w_J(R) \cdot S_J^{\mathrm{eff}}(R). \tag{4a}$$

The J-dependent opacity O_J is given by

$$O_J = \int_{R_{l_J}}^{\infty} P_J(R)\,\mathrm{d}R. \tag{6}$$

If the total autoionization width $\Gamma(R)$ is due to the decay to several exit channels k, i.e.

$$\Gamma(R) = \sum_k \Gamma_k(R), \tag{7}$$

the partial autoionization probabilities $P_J^k(R)$ are simply related to $P_J(R)$ in (4), (4a) by

$$P_J^k(R) = 2w_J^k(R) \cdot S_J^{\mathrm{eff}}(R) = [\Gamma_k(R)/\Gamma(R)] \cdot P_J(R), \tag{8}$$

where $w_J^k(R) = \Gamma_k(R)/\hbar v_J(R)$; here, $S_J^{\mathrm{eff}}(R)$ is identical to the expression given in (5), since the survival of the system is, as before, related to the total autoionization width $\Gamma(R)$. With (8) the differential cross sections $q_k(R)$ are obtained from

$$\begin{aligned} q_k(R) &= (\pi\hbar^2/2\mu\, E_{\mathrm{rel}}) \sum_{J=0}^{\infty} (2J+1)\, P_J^k(R) \\ &= [\Gamma_k(R)/\Gamma(R)]\, q(R), \end{aligned} \tag{9}$$

i.e. once $q(R)$ has been calculated, the partial $q_k(R)$ are obtained simply by multiplication of $q(R)$ with the local branching ratios $b_k(R) = \Gamma_k(R)/\Gamma(R)$.

In Fig. 4, we present the total and partial cross sections Q, Q_{6s}, Q_{6p}, and Q_{4f} as a function of relative collision energy E_{rel} in the range $10 \leq E_{\mathrm{rel}} \leq 500$ meV. All the cross sections are found to decrease with rising E_{rel}, a behaviour, which is common to Penning ionization for attractive systems [6—8, 18, 19, 22, 39, 40]. The 4f-cross sections shows a minimum around $E_{\mathrm{rel}} = 300$ meV, a behaviour, which has been observed before in energy dependent Penning ionization cross sections [7, 8, 36, 39]. The shape of the cross

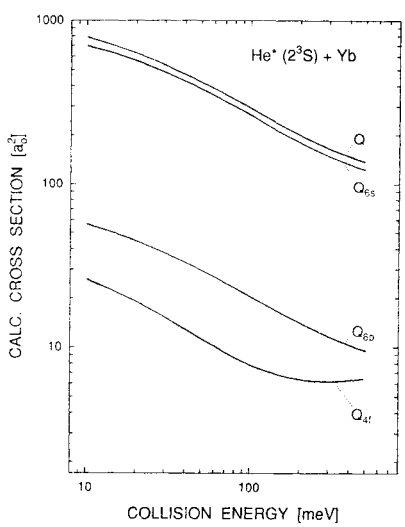

Fig. 4. Collision energy dependence of total and partial ionization cross sections Q, Q_{nl}, calculated for the system He*(2^3S) + Yb(^{1}S$_0$) with the entrance channel potential $V^*(R)$ and autoionization width functions $\Gamma_{nl}(R)$ shown in Fig. 3. nl = 6s, 6p, 4f correspond to formation of Yb$^+$(6s ^{2}S$_{1/2}$), Yb$^+$(6p ^{2}P), and Yb$^+$(4f^{13} 6s^2 ^{2}F) ions, respectively

section depends mainly on the relative slopes of the potential $V^*(R)$ and the relevant width function [39]; in the present case, it is associated with the steep slope of the partial width $\Gamma_{4f}(R)$. The branching ratios for ionization into the 6s-, 6p-, and 4f-channels, calculated for the collision energy distribution of our experiment (Table 1, $\bar{E}_{rel} =$ 66 meV), are in satisfactory agreement with the measured values (see Table 2); this indicates that our semiempirical width functions are realistic choices. We note that experimental values of absolute ionization cross sections are not available for He*(2^3S) + Yb; for the chemically similar system He*(2^3S) + Ba, however, Gérard and Hotop [41] measured both the energy dependence of the total ionization cross section $Q_{Ba}(E_{rel})$ and determined an absolute value at $E_{rel} = 0.1$ eV with the result Q_{Ba} (0.1 eV) = $196\, a_0^2$ $\left(\text{estimated uncertainty } \begin{pmatrix}+100\\-50\end{pmatrix}\%\right)$. The energy dependence of our calculated Yb-cross section Q_{Yb} is close to that measured for Q_{Ba}, and our absolute value Q_{Yb} (0.1 eV) = $298\, a_0^2$ is within the uncertainty range of Q_{Ba} (0.1 eV).

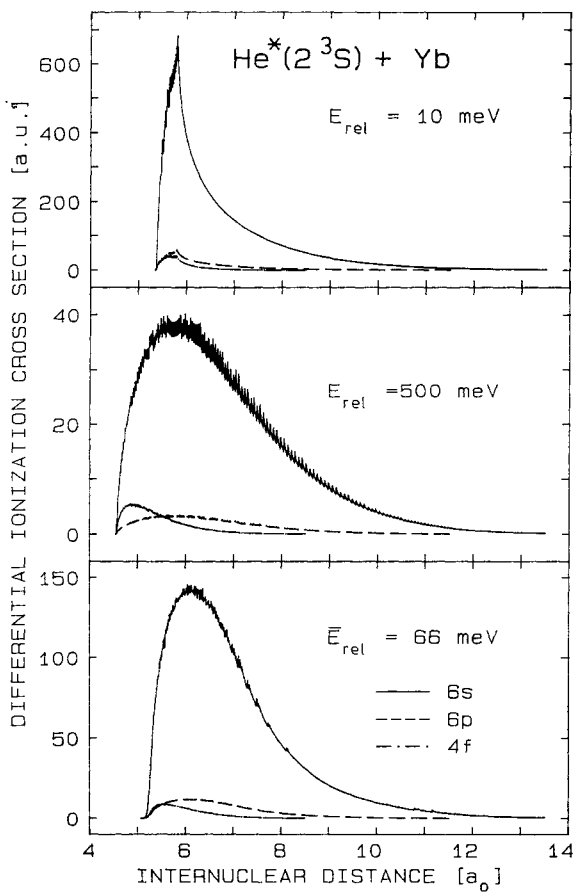

Fig. 5. Differential ionization cross sections $q_{nl}(R)$ $[a_0^2/a_0]$ for the system He*(2^3S) + Yb($^1S_0$), calculated at the two discrete collision energies $E_{rel} = 10$ meV and $E_{rel} = 500$ meV as well as for the relevant collision energy distribution of our experiment (see Table 1; $\bar{E}_{rel} = 66$ meV)

In Fig. 5, we show the partial, R-differential cross sections $q_k(R)$ for a) the discrete collision energy $E_{rel} = 10$ meV, b) for $E_{rel} = 500$ meV, and c) for a collision energy distribution appropriate for our experimental conditions (average collision energy $\bar{E}_{rel} = 66$ meV). Fig. 5 demonstrates that the 4f-channel is substantial only for $R < 7\ a_0$, whereas the 6s- and 6p-channels accumulate their cross sections over a much broader R-range. According to the repulsion of our $V^*(R)$, an increase in collision energy from 10 to 500 meV leads to a decrease in the distance of closest approach from 5.36 a_0 to 4.55 a_0 (for $J = 0$) and a corresponding relative increase of the 4f-channel cross section, as observed in Fig. 4.

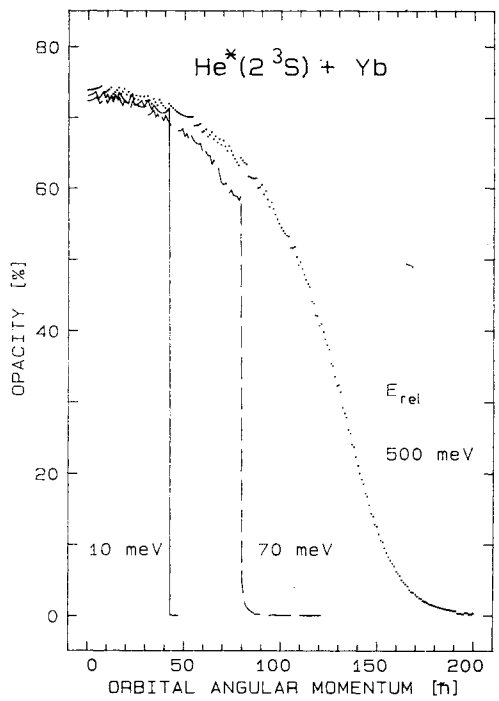

Fig. 6. Opacity functions O_J, i.e. ionization probabilities as a function of orbital angular momentum J, for the system He*(2^3S) + Yb($^1S_0$), calculated at the three discrete collision energies $E_{rel} = 10$, 70, 500 meV

In Fig. 6, we present the opacities O_J, calculated at the three discrete collision energies $E_{rel} = 10$ meV, 70 meV, and 500 meV. At $E_{rel} = 10$ meV ($E_{rel} \ll D_{e^*}$), one observes a behaviour typical for "close collision systems" [18, 29, 42]. For such systems only collisions with orbital angular momenta $J \leq J_c(E_{rel})$, which surmount the rotational barrier in the effective potential $V^*(R) + \hbar^2 J(J+1)/2\mu R^2$ and thus access close distances (where the autoionization coupling is large), contribute to ionization. At sufficiently small E_{rel}, the classical turning points R_{t_J} change little with J for $J \leq J_c$ and jump to large values for $J > J_c$; correspondingly, the opacities O_J are nearly constant for $J \leq J_c$ and close to zero otherwise. This behaviour is in essence still observed at $E_{rel} = 70$ meV ($E_{rel}/D_{e^*} \approx 0.44$), whereas for $E_{rel} = 500$ meV ($E_{rel}/D_{e^*} \approx 3$) the opacities O_J decrease smoothly, reflecting the steady increase of the turning points R_{t_J}. For low J, the opacities O_J are almost independent of the collision energy. This behaviour

is expected for $E_{rel}/D_e^* \ll 1$, since then the radial velocities in the R-range of interest are governed by the molecular attraction. For $E_{rel} \gtrsim D_e^*$, however, the radial velocities increase significantly with rising E_{rel}; the corresponding decrease in time for autoionization is, however, compensated by the penetration to smaller distances for the given entrance channel potential $V^*(R)$ and width function $\Gamma(R)$.

4. Conclusions

An electron spectrometric study of $He^*(2^3S) + Yb$ has revealed that this system presents an especially clear atomic example for the surface sensitivity of Penning ionization. In contrast to VUV photoionization of Yb, $He^*(2^3S)$ Penning ionization mainly yields $Yb^+(6s)$ ions, accompanied by about 8% correlation-induced $Yb^+(6p)$ formation and very little ($\lesssim 2.5\%$) 4f-ionization. These findings are associated with the orbital-dependent autoionization width functions $\Gamma_k(R)$, which largely reflect the electron density of the respective target electrons in the region of the He(1s) hole. Based on semiempirical local complex potentials, we have carried out classical calculations of the 6s-, 6p-, and 4f-Penning ionization cross sections, thereby shedding light on the dependence of the various cross sections and ionization probabilities on collision energy, internuclear distance, and orbital angular momentum.

Acknowledgements. This work has been supported by the Deutsche Forschungsgemeinschaft through Sonderforschungsbereich 91 "Energietransfer bei atomaren und molekularen Stoßprozessen". AJY is grateful to the SFB 91 and to the Fachbereich Physik (Universität Kaiserslautern) for their support and hospitality. We thank D. A. Shirley for permission to reproduce the HeI (58.4 nm) photoelectron spectrum of Yb (Fig. 4 in ref. [4]) in Fig. 2 of the present paper, and we gratefully acknowledge C. Kerling, N. Böwering, and U. Heinzmann for providing details of their HeI and NeI photoelectron data prior to publication. We thank M. W. Müller for a useful discussion concerning section 3.3.

References

[1] BERKOWITZ, J.: Photoabsorption, Photoionization, and Photoelectron Spectroscopy. New York: Academic Press, 1979.
[2] FROST, D. C.; MCDOWELL, C. A.; VROOM, D. A.: Chem. Phys. Lett. **1** (1967) 93.
[3] SÜZER, S.; LEE, S.-T.; SHIRLEY, D. A.: Phys. Rev. A **13** (1976) 1842.
[4] LEE, S. T.; SÜZER, S.; MATTHIAS, E.; ROSENBERG, R. A.; SHIRLEY, D. A.: J. Chem. Phys. **66** (1977) 2496.
[5] KERLING, C.; BÖWERING, N.; HEINZMANN, U.: Abstracts of Contributed Papers, XVI ICPEAC, p. 9, New York, 1989, and private Communication.
[6] HOTOP, H.: Radiation Research **59** (1974) 379.
[7] NIEHAUS, A.: Adv. Chem. Phys. **45** (1981) 399; and: Phys. Rep. **186** (1990) 149.
[8] YENCHA, A. J.: Electron Spectroscopy (C. R. Brundle and A. D. Baker, Eds.) London: Academic Press, 1984, Vol. 5, p. 197.
[9] MORGNER, H.: Comments At. Mol. Phys. **21** (1988) 195.
[10] ČERMÁK, V.; HERMAN, Z.: Chem. Phys. Lett. **2** (1968) 359.
[11] HOTOP, H.; NIEHAUS, A.: Z. Phys. **228** (1969) 68.
[12] MILLER, W. H.; MORGNER, H.: J. Chem. Phys. **67** (1977) 4923.
[13] OHNO, K.; MUTOH, H.; HARADA, Y.: J. Am. Chem. Soc. **105** (1983) 4555.
[14] DRIESSEN, J. P. J.; VAN DE WEIJER, F. J. M.; ZONNEVELD, M. J.; SOMERS, L. M. T.; JANSSENS, M. F. M.; BELJERINCK, H. C. W.; VERHAAR, B. J.: Phys. Rev. Lett. **62** (1989) 2369.
[15] MILLER, W. H.; SLOCOMB, C. A.; SCHAEFER III, H. F.: J. Chem. Phys. **56** (1972) 1347.
[16] HICKMAN, A. P.; ISAACSON, A. D.; MILLER, W. H.: J. Chem. Phys. **66** (1977) 1483.
[17] BIENIEK, R. J.: Phys. Rev. A **18** (1978) 392.

[18] WAIBEL, H.; RUF, M.-W.; HOTOP, H.: Z. Phys. D **9** (1988) 191.
[19] MERZ, A.; MÜLLER, M. W.; RUF, M.-W.; HOTOP, H.; MEYER, W.; MOVRE, M.: Chem. Phys. **145** (1990) 219.
[20] MEYER, W.; MOVRE, M.: Z. Phys. D (to be published).
[21] MERZ, A.; MÜLLER, M. W.; RUF, M.-W.; HOTOP, H.; MEYER, W.; MOVRE, M.: Chem. Phys. Lett. **160** (1989) 377.
[22] COHEN, J. S.; MARTIN, R. L.; LANE, N. F.: Phys. Rev. A **31** (1985) 152.
[23] PADIAL, N. T.; COHEN, J. S.; MARTIN, R. L.; LANE, N. F.: Phys. Rev. A **40** (1989) 117.
[24] LU, C. C.; CARLSON, T. A.; MALIK, F. B.; TUCKER, T. C.; NESTOR Jr., C. W.: Atomic Data **3** (1971) 1.
[25] BOZSO, F.; YATES, Jr., J. T.; ARIAS, J.; METIU, H.; MARTIN, R. M.: J. Chem. Phys. **78** (1983) 4256.
[26] HARADA, Y.: Surface Sci. **158** (1985) 455.
[27] KELLER, W.; MORGNER, H.; MÜLLER, W. A.: Molec. Phys. **58** (1986) 1039.
[28] WORATSCHEK, B.; SESSELMANN, W.; KÜPPERS, J.; ERTL, G.; HABERLAND, H.: Surface Sci. **180** (1987) 187.
[29] RUF, M.-W.; YENCHA, A. J.; HOTOP, H.: Z. Phys. D **5** (1987) 9.
[30] HOTOP, H.; NIEHAUS, A.: Z. Phys. **238** (1970) 452.
[31] MILLER, W. H.: J. Chem. Phys. **52** (1970) 3563.
[32] NAKAMURA, H.: J. Phys. Soc. Jpn. **26** (1969) 1473; **31** (1971) 575.
[33] JONES, R. O.: J. Chem. Phys. **72** (1980) 3197.
[34] MILLER, T. M.; BEDERSON, B.: Adv. At. Mol. Phys. **13** (1978) 1.
[35] BUCK, U.; HOPPE, H. O.; HUISKEN, F.; PAULY, H.: J. Chem. Phys. **60** (1974) 4925.
[36] HICKMAN, A. P.; MORGNER, H.: J. Phys. B **9** (1976) 1765. SISKA, P. E.: Chem. Phys. Lett. **63** (1979) 25. BURDENSKI, S.; FELTGEN, R.; LICHTERFELD, F.; PAULY, H.: Chem. Phys. Lett. **78** (1981) 296.
[37] FROESE-FISCHER, CH.: Atomic Data **4** (1972) 301.
[38] DESCLAUX, J. P.: Comp. Phys. Comm. **9** (1975) 31.
[39] ILLENBERGER, E.; NIEHAUS, A.: Z. Phys. B **20** (1975) 33.
[40] NEYNABER, R. H.: Electronic and Atomic Collisions. (N. Oda and K. Takayanagi, Eds.) Amsterdam: North Holland, 1980, p. 287.
[41] GÉRARD, K.; HOTOP, H.: Chem. Phys. Lett. **43** (1976) 175.
[42] BELL, K. L.; DALGARNO, A.; KINGSTON, A. E.: J. Phys. B **1** (1968) 18.
[43] EBDING, T.; NIEHAUS, A.: Z. Phys. **270** (1974) 43.

Bei der Redaktion eingegangen am 15. Februar 1990.

Anschr. d. Verf.: Dr. H. HOTOP,
Dr. M.-W. RUF,
Fachbereich Physik,
Universität Kaiserslautern
W-6750 Kaiserslautern, FRG

Dr. A. J. YENCHA
Department of Physics and
Department of Chemistry
State University of New York at Albany
Albany, N. Y. 12222, USA

Dr. B. FRICKE
Fachbereich Physik
Universität/GHS Kassel
W-3500 Kassel, FRG